Langmuir

ARTICLE

pubs.acs.org/Langmuir

Evolutionary Screening of Collagen-like Peptides That Nucleate Hydroxyapatite Crystals

Woo-Jae Chung,[†,§,∥] Ki-Young Kwon,[†,∥] Jie Song,[⊥] and Seung-Wuk Lee*[,†,‡]

[†]Department of Bioengineering and [‡]Berkeley Nanoscience and Nanoengineering Institute, University of California, Berkeley, Berkeley, California 94720, United States

[§]Physical Biosciences Division, Lawrence Berkeley National Laboratory, Berkeley, California 94720, United States

[∥]Department of Chemistry, Gyeongsang National University, Jinju, 660-701 South Korea

[⊥]Department of Orthopedics & Physical Rehabilitation and Department of Cell Biology, University of Massachusetts Medical School, Worcester, Massachusetts 01655, United States

Supporting Information

ABSTRACT: The biogenesis of inorganic/organic composite materials such as bone typically involves the process of templated mineralization. Biomimetic synthesis of bone-like materials therefore requires the development of organic scaffolds that mediate mineralization of hydroxyapatite (HAP), the major inorganic component of bone. Using phage display, we identified a 12-residue peptide that bound to single-crystal HAP and templated the nucleation and growth of crystalline HAP mineral in a sequence- and composition-dependent manner. The sequence responsible for the mineralizing activity resembled the tripeptide repeat (Gly-Pro-Hyp) of type I collagen, a major component of bone extracellular matrix. Using a panel of synthetic peptides, we defined the structural features required for mineralizing activity. The results support a model for the cooperative noncovalent interaction of the peptide with HAP and suggest that native collagen may have a mineral-templating function in vivo. We expect this short HAP-binding peptide to be useful in the synthesis of three-dimensional bone-like materials.

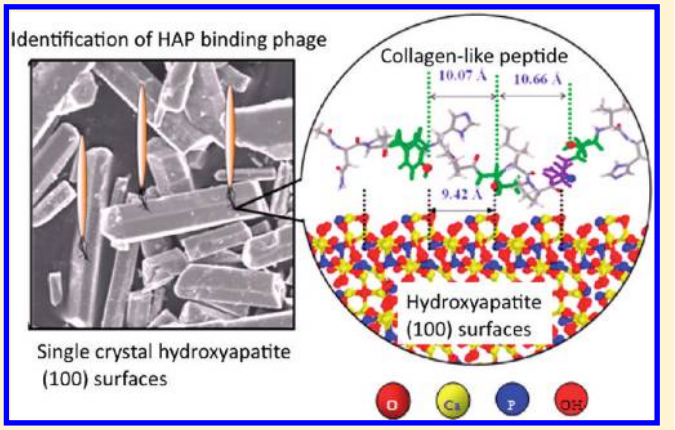

1. INTRODUCTION

Biomaterials composed of integrated inorganic and organic components possess unique properties that are difficult to replicate in a synthetic context. For example, natural bone is tough yet lightweight and fracture resistant, qualities that are derived from the integration of its primary inorganic material, hydroxyapatite (HAP) ($Ca_{10}(PO_4)_6(OH)_2$), with various proteins and extracellular matrix (ECM) components.[1,2] The formation of natural bone is thought to occur by the templated mineralization of HAP by the surrounding proteins, which include collagen and highly acidic phosphoproteins attached to the collagen scaffold.[3,4] It has been proposed that the acidic groups serve as binding sites for calcium ions and align them in an orientation that matches the HAP crystal lattice.[5] However, the biological mineralization process is not understood at a molecular level.

Considerable effort has been made to synthesize bone mimetic materials, including approaches that seek to reproduce the biological templated mineralization process.[4,6] Several groups have attempted to mineralize polymer substrates with HAP using various in vitro mineralization techniques in combination with the manipulation of polymer surface chemistries.[6−9] In nature, bone-associated proteins play important roles in templated mineralization.[2,10] These proteins possess sequences capable of nucleating HAP crystal formation, and their direct binding to HAP creates structural integration of the organic and inorganic matrices. An appealing strategy for biomimetic bone synthesis would be to employ HAP-binding peptides to facilitate HAP crystal growth. Unfortunately, the rational design of such peptides is deterred by a lack of knowledge regarding the sequences that guide HAP mineralization in vivo. Recently, various combinatorial display processes have been used to identify peptides or proteins capable of binding target materials including organic proteins[11−13] and inorganic material surfaces.[14−18] Moreover, these binding peptides have been shown to template the formation of various inorganic materials to form highly integrated composites.[14,16,17,19−25] In addition, many research groups have

Received: November 30, 2010
Revised: January 6, 2011

   dx.doi.org/10.1021/la104757g | *Langmuir* XXXX, XXX, 000–000

used phage display to identify peptides that bind to polycrystalline HAP and have reported various in vitro HAP specific binding affinities.[26−28] However, due to the complex surface structure of the polycrystalline HAP crystals used in these studies and the complexity of the mineral-protein interfaces during mineralization, the identification of the role of these peptides in the structure and function relationship of bone biosynthesis remains challenging. Therefore, a well-defined model system may help to provide insight into these complex biomineralization processes. Here, we report the identification of a novel peptide that bound to single-crystal HAP (100) surfaces and exhibited the ability to template the nucleation and growth of HAP crystals in vitro. Interestingly, the peptide, which was discovered at physiological pH (7.5), had a sequence similar to that of the major motif of type I collagen (Gly-Pro-Hyp). We also proposed structure and function relationship between identified peptides and their functions through computational modeling and further surface structure characterization.

2. EXPERIMENTAL SECTION

2.1. Materials. Ph.D.-12, -7, and -C7C Phage Display Peptide Library Kits were purchased from New England Biolabs (Ipswich, MA, USA). Tris-HCl, Glycine-HCl, NaCl, bovine serum albumin (BSA), Tween-20, and IPTG/X-gal were purchased from Sigma Aldrich (St. Louis, MO, USA). Polycrystalline HAP was obtained from Alfa Aesar Co. (Milwaukee, WI, USA). For peptide synthesis, preloaded (cysteine and biotinylated-lysine) Wang resins were purchased from Novabiochem (San Diego, CA, USA). Fmoc-amino-diethoxy-acetic acid and cleavage reagents trifluoroacetic acid, thioanisole, phenol, ethanedithiol, and tri-isopropyl silane were also obtained from Sigma Aldrich.

2.2. Single-Crystal HAP. Commercial polycrystalline HAP powders were dry-mixed with potassium sulfate at a K_2SO_4/HAP weight ratio of 1.6. The mixture was placed in a clean alumina crucible and heated in a furnace from room temperature to 1190 °C at a rate of 5 °C/min. After holding the temperature at 1190 °C for 3.5 h, the sample was cooled naturally to room temperature within the shut-off furnace. The single-crystal HAP whiskers were separated from the solidified mass by washing the mass with Milli-Q water at 90 °C three times. The whiskers were then air-dried. The aspect ratios (c:a) of these HAP single crystals were in the range of 2−18, with the median whisker diameter and length at 9 and 55 μm, respectively. We characterized surface charges of HAP crystals by measuring ζ potential using a Zetasizer Nano-ZS (Malvern Instruments Ltd., Worcestershire, UK). One milligram of HAP crystals was suspended in 1 mL of Tris-buffered saline (TBS) solution (pH 7.5) and incubated overnight. The HAP suspension was vortexed, and 0.7 mL of suspension was loaded in a ζ potential measurement cuvette (universal dip cell). The cuvette was hand-shaken and loaded. The ζ potential value was measured and processed using the Expert System (Malvern Instruments Ltd., Worcestershire, UK).

2.3. Phage Display for Selection of HAP Binding Peptide Motifs at pH 7.5. Equal amounts of three different types of commercially available phage library suspensions, 7mer, 7mer constrained, and 12mer (PhD-7, PhD-C7C, and PhD-12, New England Biolabs, MA), were mixed to generate a diverse and randomized peptide library of over 6.7×10^9 sequences. Target HAP crystals were etched with 0.2 M glycine-HCl to remove impurities prior to phage panning and stored in TBS buffer at pH 7.5 to maintain their positive charge. The combined phage libraries were incubated with 5 mg HAP crystals for 1 h using 0.1% of TBS Tween-20 (TBST) buffer. Unbound or loosely bound phages were removed by washing with TBS 10 times, and tightly bound phages were eluted with 1 mL of a 0.2 M glycine-HCl suspension (pH 2.2). The eluted phages were amplified using *Escherichia coli* cultures and purified using polyethylene glycol precipitation. This selection procedure was repeated using increasing amounts of the surfactant Tween-20 (0.2%, 0.3%, and 0.4% sequentially from second to fourth rounds). After three rounds of screening, the eluted phages were diluted and titered on the *E. coli* plates. More than 100 plagues were picked and analyzed by DNA sequencing.

In order to determine the strongest HAP binding receptors from the large subset of phage display results, the phages bearing HAP binding peptides were collected. The phage isolated from HAP phage display screening were individually picked, amplified separately, and diluted to a concentration of 10^6 pfu/μL. A single round of phage screening was performed against 5 mg of HAP in 0.1% TBST. The HAP binding phages were simultaneously exposed to the HAP target substrate in solution. After this competitive binding, the weakly bound phages were washed from the target, while the remaining strongly bound phages were eluted and titrated on LB Xgal/IPTG agar plates.[29] Phage titration was used to select phage plaques with receptor inserts.[29] Between 60 and 100 plaques, which appeared blue, were picked and sequenced to reveal the strongest binding sequences.

2.4. HAP Binding Assays. Four milligrams per milliliter of HAP crystals were incubated for 30 min with $\sim 10^{12}$ pfu/ml of CLP7, CLP12, or wild-type phages. The HAP crystals were then washed 10 times with TBS solution (pH 7.5) containing 0.5% Tween-20. The phages bound to the HAP surfaces were labeled with R-phycoerythrin-conjugated monoclonal pVIII antibody (Amersham Pharmacia Biotech, UK), and fluorescence images were acquired (Nikon fluorescence microscope, Japan). The fluorescence intensity was quantified by a FACSCalibur flow cytometer (BD Biosciences, San Jose, CA, USA). Bound phages were also eluted by 0.2 M glycine-HCl (pH 2.2) and quantified.

2.5. CLP12 and Control Peptide Synthesis. All peptides were synthesized using standard Fmoc chemistry-based solid-phase peptide synthesis[30] with amino acids and preloaded (cysteine or biotinylated-lysine) Wang resins. Resin cleavage and deprotection reactions were performed for 2 h with the cocktail of 82.5% trifluoroacetic acid, 5% thioanisole, 2.5% water, 5% phenol, 2.5% ethanedithiol, and 2.5% tri-isopropyl silane. Cleaved peptides were purified by HPLC to >95% purity.

2.6. Chemical Force Microscopy of CLP12. We measured the adhesion force of CLP12 peptide with (100) HAP crystal surfaces using chemical force microscopy techniques. We functionalized the atomic force microscopy (AFM) tip (TR400PB, Asylum Research, Santa Barbara, CA) using CLP12-GGGC peptide solution (1 mM for 2 h) based on thiol-gold chemistry. The spring constant (k) of the tip was determined on a clean silicon substrate (86 mN/m) prior to the measurement. The single-crystal HAP was deposited on a glass substrate by epoxy adhesive (12 h) as previously reported[31−33] and mounted on a flow cell (Asylum Research, Santa Barbara, CA) and washed with buffer or deionized (DI) water flow (30 mL). After stopping flow and stabilizing the system (for 1 h), chemical force curves were collected from seven randomly chosen points on flat HAP (100) surfaces (100 times per point) using the Asylum atomic force microscope MFP3D (Asylum Research, Santa Barbara, CA). The adhesion forces were measured taking two points at minimum forces and the baseline (the region where the tip was retracted far away from the sample surface) using Igor software 6.0 (WaveMetrics, Inc. Lake Oswego, OR, USA) and an Asylum software package (Asylum Research).

2.7. HAP Crystal Nucleation Assays. We characterized the nucleating ability of the identified peptide using an approach previously reported by Stupp and co-workers.[34] The synthetic peptide was dissolved in water (1.5 mg/mL), and 5 μL of aqueous peptide solution was applied to a holey carbon-coated transmission electron microscopy (TEM) grid for 2 min. The peptide-loaded TEM grid was then treated with 10 μL of 5 mM Na_2HPO_4 on one side and 10 μL of 10 mM $CaCl_2$ on the other side. After 30 min, 1 h, and 2 h, the TEM grids were washed three times in 100 μL of DI water. After drying the TEM grids thoroughly, transmission electron micrographs were taken using a JEOL-200 TEM and

dx.doi.org/10.1021/la104757g |*Langmuir* XXXX, XXX, 000–000

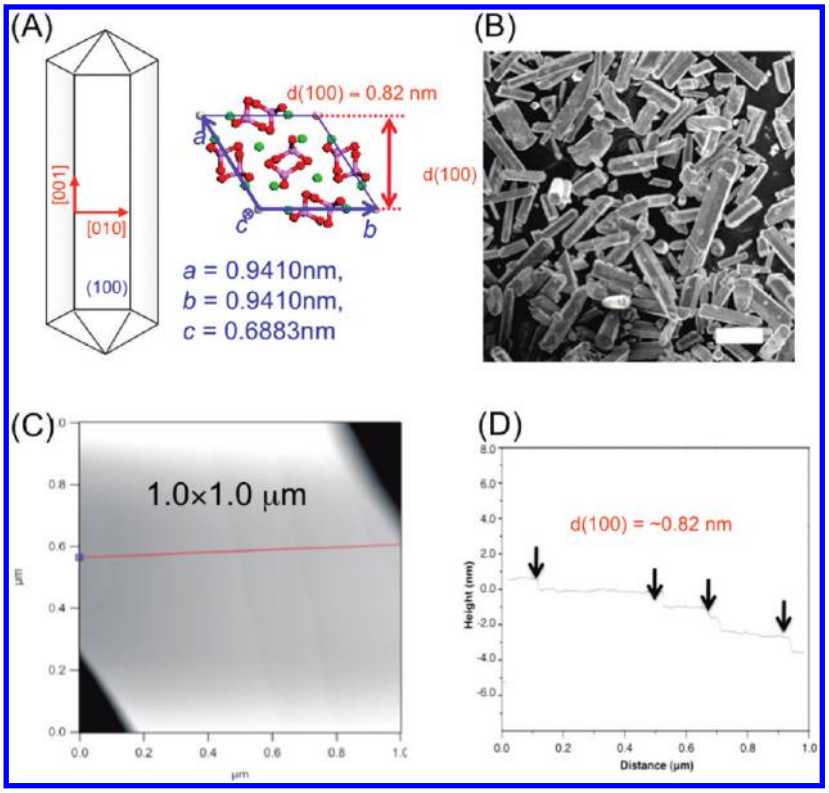

Figure 1. Structure of HAP surfaces. (A) Schematic diagram of single-crystal HAP surfaces, which are comprised mainly of (100) surfaces on their six facets, and the unit cell structures showing the unit cell height of (100) layer interspacing (0.82 nm). (B) SEM micrograph of whisker-shaped single-crystal HAP prepared by molten salt synthesis (Scale bar 20 μm). (C) AFM micrograph of (100) surface of HAP surfaces. (D) Surface profiles of HAP showing steps with $d(100)$ height.

a Philips CM200/FEG at 200 kV acceleration voltage at the National Center of Electron Microscopy (Lawrence Berkeley National Laboratories, Berkeley, CA, USA). Images were taken on film negatives or using a digital camera with a Gatan Imaging Filter (Gatan Inc., Pleasanton, CA, USA). Samples were also prepared using a similar mineralization method for scanning electron microscopy (SEM) analysis. Specifically, 1.5 mg/mL of aqueous peptide solution was applied to gold substrates for 5 min. Without removal of the suspension, 10 μL of 5 mM Na_2HPO_4 and 10 μL of 10 mM $CaCl_2$ were applied on the gold substrates, and the samples were kept in a sealed glass chamber. After 2 h, the substrates were washed three times in 100 μL DI water. After drying, SEM images were taken using a field emission environmental scanning electron microscope (FE-ESEM: Hitachi) at the Lawrence Berkeley National Laboratories (Berkeley, CA).

2.8. Computational Modeling. The possible conformational structures of the CLP12 peptide were modeled using molecular mechanics (MM) calculations. The Merck molecular force field (MMFF) and the analytical generalized-Born/surface-area (GB/SA) solvation model for water implemented in the MacroModel program (Maestro graphical user interface version 6.5.007) was used at the Chemistry Computation Facility, University of California, Berkeley (Berkeley, CA, USA).

3. RESULTS AND DISCUSSION

We synthesized single-crystal HAP using a molten salt synthesis approach.[29] The resulting crystals were elongated hexagonal rods mainly covered by six (100)-like surfaces (Figure 1A,B). SEM analysis showed that exposed flat (100) surfaces comprised ~90% of the single-crystal surface area. We observed the surface topography of the target HAP crystal using an MFP3D AFM (Asylum Research) in contact mode in situ. In buffered solution, the HAP (100) surface was dominated by atomically flat terraces separated by molecular steps (Figure 1C,D). We found that multiple steps parallel to the [001] direction were the most commonly observed. Vertical cross-sectional analysis showed that the average height of these steps was 0.84 nm ±0.10 nm, which corresponds to the interlayer distance between (100) surfaces ($d(100) \approx 0.82$ nm), as previously reported.[31,33] We measured the surface charge (ζ potential) of the HAP whiskers in pH 7.5 buffer using a Zetasizer (Malvern Instruments, UK), which gave the value of -11.45 ± 1.49 mV. Therefore, we identified peptides that specifically bound to (−) charged HAP (100) surfaces.

We employed commercial libraries of M13 bacteriophage possessing either 12mer or 7mer randomized amino acid sequences fused to their pIII coat protein (New England Biolabs). The 7mer sequences were either linear or conformationally constrained by an intramolecular disulfide bond flanking the randomized sequence. Combined, the libraries were estimated to comprise 6.7×10^9 unique sequences. Both single-crystal HAP (prepared by molten salt synthesis)[35] and commercial polycrystalline HAP were used for phage panning. Phages were selected for specific HAP binding as depicted in Figure 2A.

After several rounds of selection, the phage were sequenced, and consensus peptide motifs were identified as shown in Figure 2B. The best binding 12mer peptide (NPYHPTIPQSVH: termed CLP12) emerged after four rounds of screening and showed a periodic display of prolines (positions 2, 5, and 8) and hydroxylated residues (positions 3, 6 and 10). Compared with the dominant 7mer constrained binding peptide (CNYPTLKSC: termed CLP7C; two cysteines form a disulfide bond) isolated under the same experimental conditions, both

dx.doi.org/10.1021/la104757g |*Langmuir* XXXX, XXX, 000–000

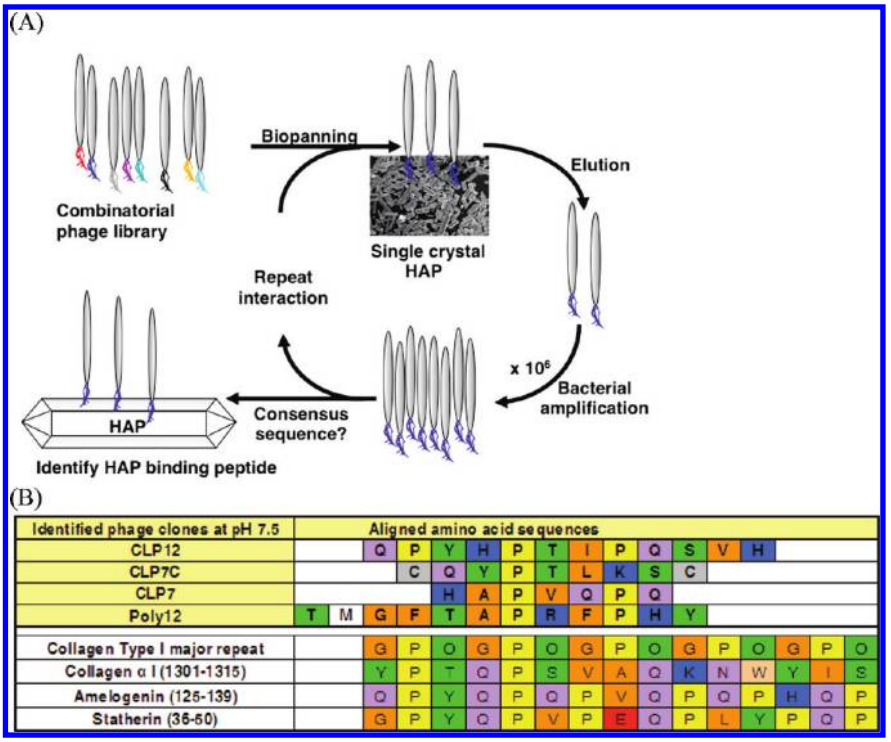

Figure 2. (A) Schematic diagram of the phage display process for the single-crystalline HAP whiskers. (B) Dominant HAP binding peptides identified from four rounds of phage display using 12mer linear, 7mer constrained, and 7mer linear peptide libraries for HAP single-crystal (100) surfaces. A 12mer linear peptide for polycrystalline HAP was also identified (upper panel). Natural bone-associated proteins, collagen type I, amelogenin, and statherin, also possess such rich [Pro-(OH)-X] tripeptide patterns (lower panel). (OH: hydroxylated amino acid residues (Ser, Thr, Tyr); X: any amino acid). Full sequence information can be found in the Supporting Information.

binding peptides exhibited remarkably conserved amino acid sequences (Asn, Tyr, Pro, Thr, Ile/Leu, and Ser). Compared with the polycrystalline HAP binding peptide (TMGFTAPRF-PHY: termed Poly12), CLP12 displayed a more regular proline repeat coupled with hydroxylated amino acid residues, which reflects the regular crystalline surfaces of HAP single crystals. Considering the absence of hydroxyproline residues in the phage libraries, the sequence similarity between the isolated peptides and the GPO repeat (in which O is hydroxyproline) frequently found in type I collagen, the major ECM protein in bone, is rather striking.

The binding affinities of isolated phages against the HAP target were visualized by fluorescence microscopy after fluorescence labeling. The relative binding affinity was quantified using flow cytometry and phage titer assays. Fluorescence images showed that considerable fluorescence was observed from CLP12 and CLP7C phages but not from wild-type phages, which did not have peptide inserts (Figure 3A−C). Corresponding fluorescence intensity measurements using flow cytometry showed that the CLP7C phage bound almost 3 times more strongly than the wild-type phage, and CLP12 showed ∼50% greater binding affinity over wild-type (Figure 3D). Binding assays using titers of phages eluted from the HAP surfaces showed similar relative binding affinities against HAP (Figure 3E). Literature suggests that constrained peptides tend to have better binding affinities than linear peptides of similar sequence.[11,36] The different lengths and amino acid compositions of CLP12 and CLP7C, however, would not allow us to ascribe their observed difference in HAP-binding affinity to variations in their structural flexibility only.

We characterized the binding affinity of the CLP12 binding peptides to HAP (100) surfaces using an Asylum atomic force microscope after modifying the AFM tip with CLP12 (Asylum Research, Santa Barbara, CA). Although the CLP7C exhibited the strongest binding affinity based on the phage binding assays, we excluded it from further characterizations by chemical force microscopy and nucleation assays due to the challenges in synthesis and functionalization of the AFM tips with CLP7C in high-purity, intact circularized form. Chemical force measurements revealed that binding of CLP12 to the (100) surfaces were pH- and solution-dependent (Figure 4). CLP12 functionalized tip force curves were collected at seven randomly chosen points on the flat HAP surface (100 times per point) in DI water. Retract curves showed very small peaks, and the histograms of the measured adhesion forces were obtained to calculate mean adhesion force and standard deviation. The value was very small and close to the detection limit. However, when the same measurements were repeated after changing the solution to pH 7.5 TBS buffer, the adhesion forces significantly increased, indicating much stronger interaction between the CLP12 peptides immobilized on the AFM tip and the HAP surface under this condition. The force histogram showed a Gaussian distribution (Figure S2, Supporting Information), and the mean adhesion force value was 554.23 ± 89.69 pN. When TBS buffer at pH 9 was used, the histogram shifted to lower range, resulting in a much lower mean adhesion force value of 97.57 pN. Upon exposure to pH 6 TBS, the HAP began to dissolve rapidly, and many pits with molecular steps were created on the (100) surfaces. Therefore, we could not establish a reliable adhesion curve under acidic pH conditions. We performed additional experiments using bare gold tips and tips modified with control peptide (Gly-Gly-Gly with acetic anhydride at the N-terminus) in pH 7.5 TBS buffer, which gave adhesion force values of

dx.doi.org/10.1021/la104757g |*Langmuir* XXXX, XXX, 000–000

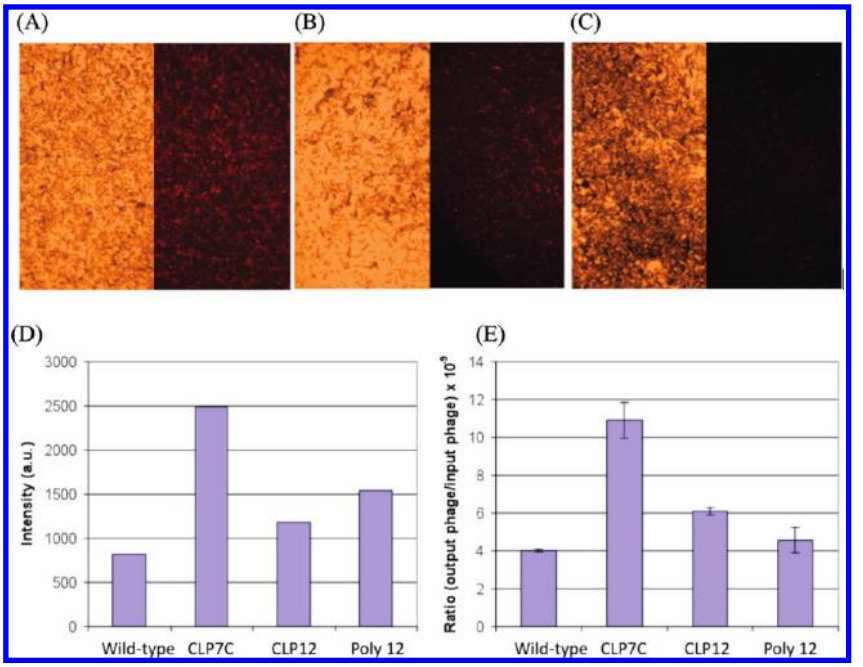

Figure 3. Optical and fluorescence micrographs of HAP crystals bound with (A) CLP7C phage, (B) CLP12 phage, and (C) wild-type phage. The quantification of bound phage using (D) cytometry and (E) phage titering.

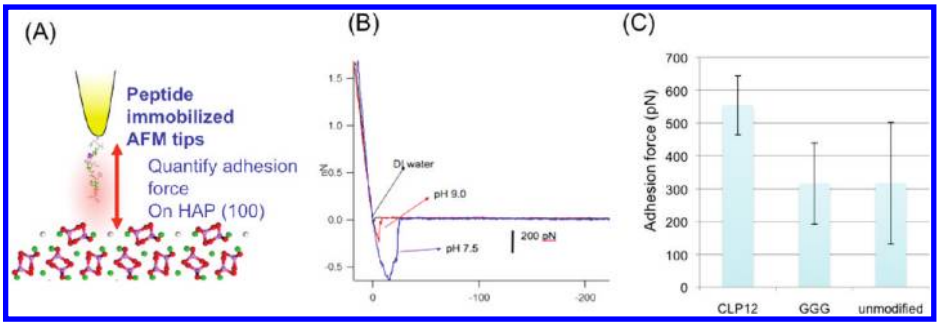

Figure 4. Chemical force measurement of CLP12 and HAP surfaces. (A) Schematic diagram of chemical force microscopy to measure the adhesion force between a single-crystal (100) HAP surface and a CLP12 peptide immobilized on an AFM tip. (B) Representative pH-dependent adhesion force curves of CLP12 adhesion on (100) HAP surfaces measured at pH 7.5, 9.0, and in DI water. (C) Adhesion force measurements of CLP12 and controls (GGG peptide and unmodified AFM tip) at pH 7.5.

317.74 ± 184.99 pN and 316.09 ± 123.59 pN, respectively, and very broad distributions. These results confirmed the specific binding of CLP12 to the (100) surfaces at pH 7.5.

The HAP-nucleating ability of the isolated peptide sequences was tested using a synthetic CLP12 peptide conjugated to a biotin linker (Gly-Gly-Gly-Lys(biotin)) on the C terminus. After incubating the CLP12 peptide (1.5 mg/mL) on a holey carbon TEM grid for 30 min with precursor Ca^{2+} and HPO_4^{2-} ions, the deposition of amorphous calcium phosphate was observed (Figure S3A, Supporting Information). After 1 h, 20−50 nm HAP crystals began to form, as evidenced by TEM micrographs and selected area electron diffraction (SAED) patterns matching those of crystalline HAP (Figure S3B). Two hours later, fully developed HAP crystals were observed throughout the TEM grids (Figure 5A). SAED showed clear ring patterns from (002), (211), and (004) plains, which are characteristic of well-crystallized HAP (Figure 5B). Energy dispersion X-ray spectroscopy (EDS) of the HAP crystals showed a Ca/P ratio of 1.67 (Figure 5C), matching the theoretical ratio of HAP. Peptide concentration-dependent nucleation was observed using a higher concentration (15 mg/mL) peptide suspension (Figure 5D). At a higher magnification, TEM micrographs revealed that the plate-like HAP minerals showed clear lattice fringed structures composed of ∼20 nm randomly oriented HAP nanocrystals (Figure 5E). An SEM micrograph of the plate-like HAP minerals templated by the peptides on a gold substrate (Figure 5F) clearly showed the three-dimensional structures of the fully grown HAP crystals. The control mineralization experiment without peptide both on the TEM grid and gold substrate did not form any crystal under identical conditions (Figure S3C).

Five control peptides (Table 1), NIYHPTPPQSVH (termed PxI), NPDHPDIPQDVH (termed OH2D), NPAHPAIPQAVH (termed OH2A), APYHPTIPASVH (termed NH2A), and NPYAPTIPQSVA (termed HIS2A), were synthesized and tested to show that CLP12 could template the nucleation and growth of HAP in a sequence- and composition-specific manner. HAP mineralization templated by peptide PxI, which contained a single displacement between proline (position 2) and isoleucine (position 7), yielded amorphous calcium phosphate deposition without any clear SAED patterns (Figure S4A). The OH2D peptide,

dx.doi.org/10.1021/la104757g |*Langmuir* XXXX, XXX, 000–000

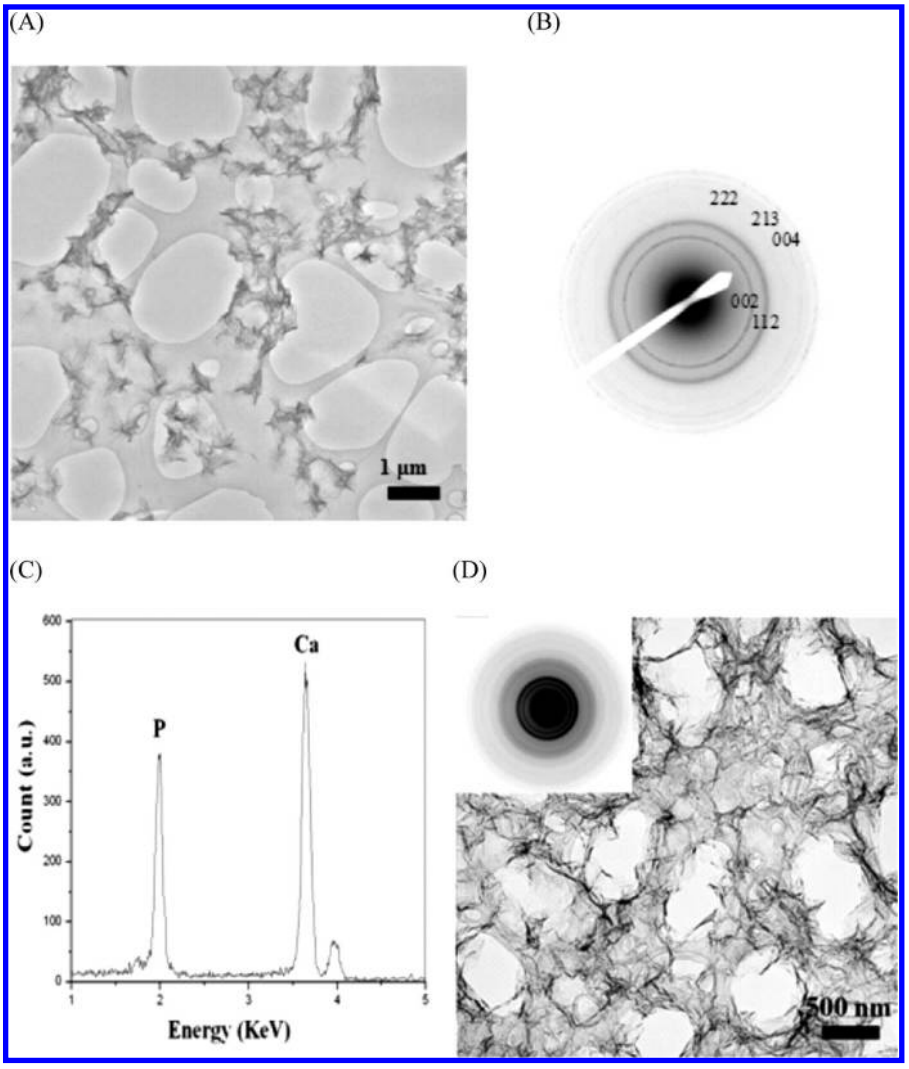

Figure 5. Electron microscopy analysis of HAP crystals mineralized using a CLP12 peptide. (A) TEM micrograph of CLP12-templated HAP crystals grown on a holey carbon film-coated Cu grid. (B) SAED pattern from image A showing a characteristic diffraction pattern, corresponding to major 002, 211, 004 planes with minor ring patterns, of crystalline HAP. (C) EDS spectrum with a Ca/P ratio of 1.67. (D,E) High-resolution TEM micrographs showing lattice fringed structures of HAP. (F) SEM micrograph of HAP crystals nucleated on a Au substrate.

Table 1. Comparison of Nucleation Ability of Control Peptides

Control peptide sequences	Nucleation ability[a]
NPYHPTIPQSVH-GGGK-biotin: CLP12 peptide	++
NI**Y**HPT**P**PQSVH-GGGK-biotin: switch P and I (PxI)	−
NP**D**HP**D**IPQ**D**VH-GGGK-biotin: switch Y, T and S to D (OH2D)	−
NPY**A**PTIPQSV**A**-GGGK-biotin: switch H to A (HIS2A)	−
APYHPTIPA**A**SVH-GGGK-biotin: switch N and Q to A (NH2A)	−
NPA**A**HPA**A**IPQ**A**VH-GGGK-biotin: switch Y, T and S to A (OH2A)	+

[a] ++: nucleation of HAP observed in 2 h; +: reduced nucleation of HAP observed in 2 h; −: nucleation of HAP not observed in 2 h.

in which the hydroxyl residues of CLP12 were substituted with aspartic acid, also induced only amorphous deposition of calcium phosphate within the 2 h (Figure S4B). Three alanine-substituted control peptides (OH2A, NH2A, and HIS2A) showed that histidine and amine residues were more critical than hydroxyl residues in templating the nucleation of crystalline HAP. The histidine- and amide-substituted peptides did not show any crystalline HAP formation (Figures S5A and S5B), but the hydroxyl residue deficient peptide showed reduced HAP-nucleation ability, with the resulting HAP crystal growth exhibiting different crystal morphologies (Figures S5C and S5D). Proline displacement and alanine substitutions caused three-dimensional conformational changes of the peptide (as suggested by MM simulations, data not shown), hence reducing the ability of the peptide to bind to HAP crystals and recruit ions for nucleation. We believe that the spatial position of each amino acid residue

dx.doi.org/10.1021/la104757g |*Langmuir* XXXX, XXX, 000–000

plays an important role in HAP nucleation activity. The comparison of the nucleation activities of these control peptides were summarized in Table 1.

It is well-known that noncollagenous ECM proteins in calcified tissues, such as sialoprotein, dentin, and amelogenin, are rich in phosphoserine, aspartate, and glutamate residues.[5,37,38] These anionic residues are believed to enrich and bind to calcium ions and template the initial formation of amorphous minerals, which subsequently ripen into more stable crystalline apatites (22−23). Our current study identified positively charged peptides that bind to negatively charged single-crystalline HAP surfaces at pH 7.5 through phage display, indicating that positively charged residues can also template HAP-mineralization under physiological conditions. Furthermore, these collagen-like short peptides are encoded with compositional and crystallographic information that epitaxially matches the HAP crystal lattice. This feature might lower the activation energy for the peptide−HAP interfacial binding event. Cooperative interactions of hydrogen bonding, van der Waals interactions, and Coulombic interactions between the isolated peptides and the HAP surfaces are likely to contribute to the specific nucleation and binding events observed.

4. DISCUSSION

Single-crystal HAP has two distinct surfaces: (100) and (010), which are identical and dominantly cover the HAP crystal surfaces.[39] The crystal growth rate through the (001) face is greater than that through the (100) face, resulting in the elongated whisker-shape of the crystal. HAP possesses dynamic surfaces in aqueous systems switching its surface charges depending on pH conditions.[40] The pI (isoelectric point) of HAP is ~pH 7 but varies depending on the measurement methods. Previous surface charge measurements using ζ potential[41] and surface charge titrations[40] of HAP crystals have shown that HAP has slightly negatively charged surfaces at physiological pH (7.4). In addition, previous high-resolution surface profiling using X-ray scattering[42] and TEM experiments[43] showed that the outer layer of HAP was composed of phosphate. Recently, we reported the surface structure of (100) HAP and its dissolution behavior, which is highly dependent on the surface structure.[31−33] When we measured the surface height profiles between pH 5.5 to 11.5, we observed profiles with only one height, corresponding to the d(100) height step (d = 0.82 nm). This result indicates that single-crystal HAP (100) surfaces are covered by a slightly negatively charged, deprotonated-phosphate layer.

Through phage display, we discovered HAP-specific peptides that interact with the HAP single-crystal (100) and identified collagen-like peptide sequences. Through AFM imaging at pH 7.5, the single crystal exhibited very stable flat surfaces, mainly composed of (100) surfaces. Therefore, we believe that CLP12 specifically interacts with the deprotonated-phosphate surface layer of (100) HAP. The conformation of CLP12 was investigated using circular dichroism (CD) spectroscopy. The CD results showed that CLP12 possessed random coil conformation. There was no difference in the CD spectra before and after calcium addition, suggesting that the conformation of the peptide did not change upon addition of calcium, and there was no calcium-induced assembly or aggregation of peptides (data not shown). CD spectra of CLP12 (0.13 mM) with different calcium ion concentrations from 1 to 100 equiv (with respect to CLP12) confirmed the finding. Other control peptides also exhibited similar behavior in their CD spectroscopy, suggesting random coil conformation. The lowest energy conformation of CLP12 in an aqueous solution was modeled using MM simulations. The distances between the oxygen atoms in the hydroxylated residues were 10.66 Å ($O_{Thr6}-O_{Ser10}$) and 10.07 Å ($O_{Thr6}-O_{Tyr3}$). These distances closely matched those between alternating hydroxyproline residues in collagen peptides (10.10 ± 0.84 Å).[44] Considering the rotational flexibility of the C−OH bonds in the hydroxylated amino acid side chains, these distances were commensurate with the unit cell distance of single-crystal HAP on the (100) face (9.42 Å) (Figure 6). At pH 7.5, the outer surface of the single-crystal (100) HAP phosphate layer was deprotonated and possessed net negative charges (ζ potential value of our single-crystal HAP: −11.45 ± 1.49 mV). On the basis of our phage display results and surface characterization of single-crystal HAP surfaces, we hypothesize that both the hydrogen bonding between the phosphates of HAP and the hydroxyl residues of the peptides, the Coulombic interaction between (−) charged HAP surfaces, and the positively charged amino acid residue (histidines) collectively contribute to the interfacial binding event.

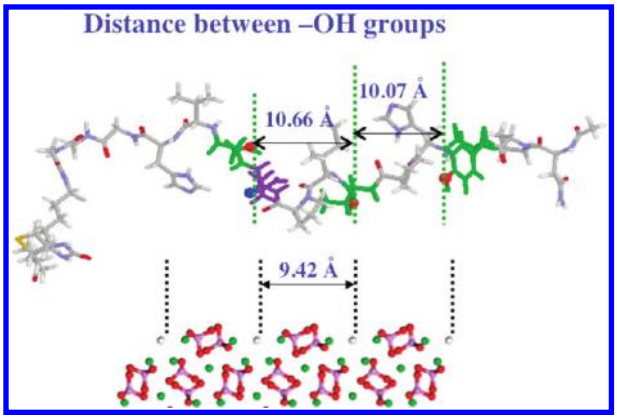

Figure 6. A model of the proposed interaction of CLP12 with the single-crystalline HAP surface, showing closely matched distances between adjacent hydroxyl residues and the HAP crystal lattice. The periodic proline and hydroxyl residues (Tyr, Thr, and Ser in green, oxygens of hydroxyl side chains in red) resemble the type I collagen repeat sequence. MM calculations were performed using the MMFF force field and the analytical GB/SA solvation model for water implemented in the MacroModel program (Maestro graphical user interface version 6.5.007). Color code for HAP lattice: Ca, green; P, purple; O, red.

Collagen extracts from many calcified matrices, dentin protein, sialoprotein, and their mimicking matrices, have been intensively studied and used for the fabrication of bone-like and dentin-like biocomposites for regenerative medicine.[38,45−47] In addition, aspartic acid- or amine group-modified self-assembled monolayers[48,49] and self-assembled fibers have been used to nonspecifically template the nucleation of HAP minerals.[4,50] However, a lack of understanding of nucleation on the molecular level and of the long encrypted protein sequences in natural hard tissues has led to the arbitrary choices of amino acid in these studies and hindered the development of more effective regenerative tissue engineering approaches. The use of short HAP-binding peptides identified in this work directly addresses the question of which amino acid sequences are most critical and sufficient for binding to and templating HAP nucleation and growth. These short peptides may be incorporated into three-dimensional polymer scaffolds to induce the nucleation of HAP crystals and generate improved artificial bone

dx.doi.org/10.1021/la104757g |Langmuir XXXX, XXX, 000–000

implants. These peptides may also be applied at the nucleation front to inhibit the growth of HAP when the overgrowth of apatites is undesirable.

5. CONCLUSION

We identified (100) single-crystal HAP binding peptides using phage display. The resulting consensus sequence resembled the tripeptide repeat (Gly-Pro-Hyp) of type I collagen, a major component of bone ECM. The peptide also exhibited nucleation activity of HAP crystals. Using a panel of synthetic peptides, we defined the structural features required for mineralizing activity. The results support a model for the interaction of the peptides with HAP through collective noncovalent interactions and suggest that native collagen may have a mineral-templating function in vivo. We expect these short HAP-binding peptides to be useful in the synthesis of three-dimensional bone-like materials.

■ ASSOCIATED CONTENT

Supporting Information. HAP binding peptides identified through phage display after fourth round of screening; AFM micrographs showing seven different measurement spots for (100) HAP surfaces, their force−distance curves, and force histograms for CLP12 peptides; and TEM micrographs for samples in which HAP was nucleated for 30 min and 1 h, the holey carbon coated TEM grid from the control mineralization experiment without peptides, control HAP mineralization templated by PxI and OH2D peptides, and HAP mineralization templated by alanine-substituted control peptides OH2A, HIS2A, and NH2A. This material is available free of charge via the Internet at http://pubs.acs.org.

■ AUTHOR INFORMATION

Corresponding Author
*E-mail: leesw@berkeley.edu.

■ ACKNOWLEDGMENT

We thank Dr. Carolyn Bertozzi for helpful discussions and support of this research. This work was supported by the National Science Foundation Early Career Development Award (DMR-0747713) and an NIH R-21 award (DE 018360-02), start-up funds from the Nanoscience and Nanotechnology Institute at the University of California, Berkeley (S.-W.L.), and the Laboratory Directed Research and Development fund from the Lawrence Berkeley National Laboratory.

■ REFERENCES

(1) Kay, M. I.; Young, R. A. *Nature* **1964**, *204*, 1050.
(2) Weiner, S.; Wagner, H. D. *Annu. Rev. Mater. Sci.* **1998**, *28*, 271.
(3) Traub, W.; Arad, T.; Weiner, S. *Proc. Natl. Acad. Sci. U.S.A.* **1989**, *86*, 9822.
(4) Hartgerink, J. D.; Beniash, E.; Stupp, S. I. *Proc. Natl. Acad. Sci. U.S.A.* **2002**, *99*, 5133.
(5) George, A.; Bannon, L.; Sabsay, B.; Dillon, J. W.; Malone, J.; Veis, A.; Jenkins, N. A.; Gilbert, D. J.; Copeland, N. G. *J. Biol. Chem.* **1996**, *271*, 32869.
(6) Song, J.; Saiz, E.; Bertozzi, C. R. *J. Am. Chem. Soc.* **2003**, *125*, 1236.
(7) Murphy, W. L.; Mooney, D. J. *J. Am. Chem. Soc.* **2002**, *124*, 1910.
(8) Liu, Q.; de Wijn, J. R.; Blitterswijk, C. A. v. *J. Biomed. Mater. Res.* **1998**, *40*, 257.
(9) Du, C.; Falini, G.; Fermani, S.; Abbott, C.; Moradian-Oldak, J. *Nat. Biotechnol.* **2003**, *21*, 513.
(10) Weiner, S.; Addadi, L. *J. Mater. Chem.* **1997**, *7*, 689.
(11) Ho, K. L.; Yusoff, K.; Seow, H. F.; Tan, W. S. *J. Med. Virol.* **2003**, *69*, 27.
(12) Petrenko, V. A.; Smith, G. P.; Mazooji, M. M.; Quinn, T. *Protein Eng.* **2002**, *15*, 943.
(13) Smith, G. P.; Petrenko, V. A. *Chem. Rev.* **1997**, *97*, 391.
(14) Sarikaya, M.; Tamerler, C.; Jen, A. K. Y.; Schulten, K.; Baneyx, F. *Nat. Mater.* **2003**, *2*, 577.
(15) Whaley, S. R.; English, D. S.; Hu, E. L.; Barbara, P. F.; Belcher, A. M. *Nature* **2000**, *405*, 665.
(16) Lee, S.-W.; Mao, C.; Flynn, C. E.; Belcher, A. M. *Science* **2002**, *296*, 892.
(17) Naik, R. R.; Stringer, S. J.; Agarwal, G.; Jones, S. E.; Stone, M. O. *Nat. Mater.* **2002**, *1*, 169.
(18) Kase, D.; Kulp, J. L.; Yudasaka, M.; Evans, J. S.; Iijima, S.; Shiba, K. *Langmuir* **2004**, *20*, 8939.
(19) Mao, C.; Solis, D. J.; Reiss, B. D.; Kottmann, S. T.; Sweeney, R. Y.; Hayhurst, A.; Georgiou, G.; Iverson, B.; Belcher, A. M. *Science* **2004**, *303*, 213.
(20) Wong Po Foo, C.; Patwardhan, S. V.; Belton, D. J.; Kitchel, B.; Anastasiades, D.; Huang, J.; Naik, R. R.; Perry, C. C.; Kaplan, D. L. *Proc. Natl. Acad. Sci. U.S.A.* **2006**, *103*, 9428.
(21) Lee, S. W.; Mao, C. B.; Flynn, C. E.; Belcher, A. M. *Science* **2002**, *296*, 892.
(22) Mao, C.; Flynn, C. E.; Hayhurst, A.; Sweeney, R.; Qi, J.; Georgiou, G.; Iverson, B.; Belcher, A. M. *Proc. Natl. Acad. Sci. U.S.A.* **2003**, *100*, 6946.
(23) Mao, C.; Liu, A.; Cao, B. *Angew. Chem., Int. Ed. Engl.* **2009**, *48*, 6790.
(24) Mao, C. B.; Solis, D. J.; Reiss, B. D.; Kottmann, S. T.; Sweeney, R. Y.; Hayhurst, A.; Georgiou, G.; Iverson, B.; Belcher, A. M. *Science* **2004**, *303*, 213.
(25) Sweeney, R. Y.; Mao, C.; Gao, X.; Burt, J. L.; Belcher, A. M.; Georgiou, G.; Iverson, B. L. *Chem. Biol.* **2004**, *11*, 1553.
(26) Gungormus, M.; Fong, H.; Kim, I. W.; Evans, J. S.; Tamerler, C.; Sarikaya, M. *Biomacromolecules* **2008**, *9*, 966.
(27) Segvich, S. J.; Smith, H. C.; Kohn, D. H. *Biomaterials* **2009**, *30*, 1287.
(28) Weiger, M. C.; Park, J. J.; Roy, M. D.; Stafford, C. M.; Karim, A.; Becker, M. L. *Biomaterials* **2010**, *31*, 2955.
(29) Whaley, S. R.; English, D. S.; Hu, E. L.; Barbara, P. F.; Belcher, A. M. *Nature* **2000**, *405*, 665.
(30) Grun, J.; Revell, J. D.; Conza, M.; Wennemers, H. *Bioorg. Med. Chem.* **2006**, *14*, 6197.
(31) Kwon, K.-Y.; Wang, E.; Chung, A.; Chang, N.; Lee, S.-W. *J. Phys. Chem. C* **2009**, *113*, 3369.
(32) Kwon, K. Y.; Wang, E.; Chang, N.; Lee, S. W. *Langmuir* **2009**, *25*, 7205.
(33) Kwon, K. Y.; Wang, E.; Chung, A.; Chang, N.; Saiz, E.; Choe, U. J.; Koobatian, M.; Lee, S. W. *Langmuir* **2008**, *24*, 11063.
(34) Hartgerink, J. D.; Beniash, E.; Stupp, S. I. *Science* **2001**, *294*, 1684.
(35) Tas, A. C. *J. Am. Ceram. Soc.* **2001**, *84*, 295.
(36) O'Neil, K. T.; Hoess, R. H.; Jackson, S. A.; Ramachandran, N. S.; Mousa, S. A.; DeGrado, W. F. *Proteins: Struct., Funct., Genet.* **1993**, *14*, 509.
(37) Weiner, S.; Veis, A.; Beniash, E.; Arad, T.; Dillon, J. W.; Sabsay, B.; Siddiqui, F. *J. Struct. Biol.* **1999**, *126*, 27.
(38) Du, C.; Falini, G.; Fermani, S.; Abbott, C.; Moradian-Oldak, J. *Science* **2005**, *307*, 1450.
(39) Kay, M. I.; Young, R. A.; Posner, A. S. *Nature* **1964**, *204*, 1050.
(40) Harding, I. S.; Rashid, N.; Hing, K. A. *Biomaterials* **2005**, *26*, 6818.
(41) Somasundaran, P.; Wang, Y. H. C. *Surface Chemical Characteristics and Adsoption Propoerties of Apatite*; Plenum Press: New York, 1984.

(42) Park, C. Y.; Fenter, P.; Zhang, Z.; Cheng, L. W.; Sturchio, N. C. *Am. Mineral.* **2004**, *89*, 1647.
(43) Sato, K.; Kogure, T.; Iwai, H.; Tanaka, J. *J. Am. Ceram. Soc.* **2002**, *85*, 3054.
(44) Bella, J.; Eaton, M.; Brodsky, B.; Berman, H. M. *Science* **1994**, *266*, 75.
(45) Zhang, W.; Liao, S. S.; Cui, F. Z. *Chem. Mater.* **2003**, *15*, 3221.
(46) He, G.; Dahl, T.; Veis, A.; George, A. *Nat. Mater.* **2003**, *2*, 552.
(47) Tye, C. E.; Rattray, K. R.; Warner, K. J.; Gordon, J. A. R.; Sodek, J.; Hunter, G. K.; Goldberg, H. A. *J. Biol. Chem.* **2003**, *7*, 7949.
(48) Zhu, P.; Masuda, Y.; Koumoto, K. *J. Colloid Interface Sci.* **2001**, *243*, 31.
(49) Rautaray, D.; Mandal, S.; Sastry, M. *Langmuir* **2005**, *21*, 5185.
(50) Sone, E. D.; Stupp, S. I. *J. Am. Ceram. Soc.* **2004**, 12756.